

# A unified approach to simulate the creep-fatigue crack growth in P91 steel at elevated temperature under SSY and SSC conditions

Marcello A. Lepore<sup>a,\*</sup>, Angelo R. Maligno<sup>a</sup>, Filippo Berto<sup>b</sup>

<sup>a</sup> *Institute for Innovation in Sustainable Engineering, University of Derby, Derby, UK*

<sup>b</sup> *Department of Mechanical and Industrial Engineering, NTNU, Richard Birkelands vei 2b, 7491 Trondheim, Norway*

---

## A B S T R A C T

The Finite Element (FE) model of a Compact Tension (C(T)) specimen, made of P91 steel with different values of loading conditions and holding times, has been chosen for simulating the creep-fatigue crack propagation in high temperature (625 °C). Two FE-based commercial software have been used considering both the Small-Scale Yielding (SSY) and the Small-Scale Creep conditions (SSC) so that Low Cycle Fatigue (LCF) properties and the C(t) integral have been used to perform the numerical simulations of creep-fatigue crack propagation. Hence, the elastic-plastic material behaviour of P91 steel has been modelled by means of the Ramberg-Osgood equation while the creep behaviour has been modelled with the Norton's model. To calculate numerically the crack growth rates for the creep-fatigue crack propagation, a modified version of the UniGrow model has been adopted also considering the creep-fatigue interaction. Finally, numerical and the experimental results available in the literature have been compared with each other. This work presents a general methodology for the simulation of the creep-fatigue phenomenon. The method can also be applied to structural components with complex geometry and challenging load conditions.

---

## 1. Introduction

The P91 steel is widely used in structural components for power generation and aircraft engine industries such as steam headers, steam turbines, gas turbines, and nuclear reactors [1,2] due to its creep strength at temperatures above 500 °C. The American Society for Testing and Materials (ASTM) has indicated this steel as P91 meaning the prefix corresponds to piping applications. The structural components made of P91 steel typically operate at high steam pressures and temperatures under a combination of cyclic loading conditions with long hold times under sustained stress. Thus, it should be desirable to increase its maximum operating temperature up to 625–650 °C to increase the energy efficiency of ultra-super critical power plants [3,4].

Failures due to creep can be classified either as resulting from widespread creep damage or resulting from localized creep damage. The structural components, which can be damaged by widespread creep, are those that are typically subjected to uniform temperatures and stress during service, such as thin-wall pipes. The creep-fatigue damage is essentially due to the fatigue and creep damage. The fatigue damage in metals is related to fatigue crack propagation while the creep damage is related to the coalescence of creep cavities.

The Creep Fatigue Crack Growth (CFCG) behaviour of engineering alloys have been investigated by a few researchers [1,5–7]. Several researchers simulated by FEM the creep crack growth behaviour using damage models [8–11,38,39]. Lu et al. [5] investigated the effect of temperature and hold time on the CFCG behaviour of a nickel-based superalloy showing that as the hold time increase, the

---

\* Corresponding author.

## Nomenclature

A, B	surface break-through points
A'	Norton creep constant
a	crack length
a <sub>0</sub>	notch length
(B)	BISS laboratory
B'	thickness of C(T) specimen
b	fatigue strength exponent
C	middle position break-through point
C(t)	C-integral
C*	creep power-law exponent
C'	Unigrow law parameter
c	fatigue ductility exponent
CFCG	creep fatigue crack growth
C(T)	compact tension specimen
D	creep power-law coefficient
d <sub>s</sub>	arc length along the contour
E	Young's modulus
EPFM	elastic plastic fracture mechanics
ERR	energy release rate
EC	extensive creep
FCG	fatigue crack growth
f <sub>conv</sub>	conversion factor
FE	finite element
FEM	finite element method
h <sub>t</sub>	hold time
HRR	Hutchinson, Rice, Rosengren singularity field
I <sub>m</sub>	constant of HRR-type stress fields
J	J-integral
K	stress intensity factor
K'	cyclic strength coefficient
K <sub>eff</sub>	effective stress intensity factor
K <sub>max</sub>	maximum value of stress intensity factor
K <sub>max,tot</sub>	total value of K <sub>max</sub>
LCF	low cycle fatigue
LEFM	linear elastic fracture mechanics
n <sub>j</sub>	outward normal of $\Gamma$
m	Norton creep exponent
NSWA	approximate crack growth model
n	strain hardening exponent
n'	cyclic hardening exponent
p, $\gamma$	UniGrow exponents
r	distance from the crack tip
R	stress ratio
rotX, rotY	model constraints
rotZ	model constraints
RP <sub>1</sub> , RP <sub>2</sub>	reference points
SIF	stress intensity factor
SSC	small scale creep
SSY	small scale yielding
T <sub>i</sub>	component of traction vector
t	time
TC	transition creep
u <sub>i</sub>	displacement vector component
u <sub>1</sub> , u <sub>2</sub> , u <sub>3</sub>	model constraints
UniGrow	unified two-parameter FCG model
VCE	virtual crack extension
(W)	Westmoreland laboratory
W	width of the C(T) specimen

crack growth behaviour changed from cycle dependent to time dependent behaviour. This transition occurred at a smaller hold time as the test temperature was increased. However, based on the work of Taira [12], the most of investigations considered the creep-fatigue damage by simply adding the fatigue and creep together. Jing et al. [13] proposed a creep-fatigue crack growth model considering the Lagneborg [14] creep-fatigue interaction term. In this work numerical investigations by FEM approach has been carried out. Numerical simulations have been based on the experimental tests of CFCG on P91 steel by Narasimhachary and Saxena, available in the literature [1]. Thus, simulations of CFCG have been performed on compact tension specimen, C(T), at a temperature of 625 °C for a hold time of 0 s, 60 s and 600 s, respectively. The proposed creep-fatigue crack propagation law is the combination of “modified” two-scale model Unigrow [34,35] which is able to detect the fatigue damage ahead of the crack front both at micro- and macro- scale level; the time-dependent law NSWA [33], which allows the calculation of the creep crack propagation and, a the time-dependent law Lagneborg’s term [14]. This is needed to calculate the creep-fatigue interaction.

## 2. Theoretical background

The SSY is both “hypothesis” and “condition” [15,18]. The “hypothesis” is at the basis of the Linear Elastic Fracture Mechanics (LEFM) while the “condition” can be considered or as an extension of LEFM. However, some authors consider the SSY as the starting point of the Elastic Plastic Fracture Mechanics (EPFM) [16,17]. In the EPFM, the Hutchinson-Rice-Rosengren (HRR) singularity is considered; however, special crack tip elements for modelling this singularity are yet to be established. The computational strategy to EPFM aims to achieve a  $1/r$  singularity. This is done by not-collapsing the nodes at the crack tip of a 20-node hexahedral element unlike the LEFM. Moreover, the mid-side nodes of the element will retain their mid position. This approach is used in Zencrack [27]. Furthermore, considering that P91 steel exhibits a hardening exponent  $n > 10$ , the asymptotic behaviour approaches ideal plastic equations [16].

Brocks considers the SSY condition as an extension of LEFM [18] and thus, the Energy Release Rate (ERR) is equivalent to the stress intensity factor (SIF) because in the SSY the equation  $J = K^2/E$  is still valid [18–20]. Differently by LEFM approach, in SSY condition the material yielding is considered and thus, taking into account the Irwin’s theory in which a fictitious crack extension used for estimating the plastic zone size,  $a_{eff}$ , and the corresponding effective SIF,  $K_{eff}$ , can be obtained [18]. If the SSY conditions are maintained during the initial loading, elastic stress and deformation fields is controlled by  $K$ . If extensive plastic deformation occurs during initial loading,  $K$  loses its significance as the dominating crack tip parameter. Under such conditions, the crack tip stresses and strains are characterized by the  $J$ -integral. At elevated temperature the stresses near the crack tip begin to relax due to creep deformation and the size of the relaxation (or creep) zone increases with time if the crack is assumed to remain stationary [21].

If the creep zone is small,  $K$  or  $J$  will continue to characterize the crack tip stresses outside the creep zone and the creep conditions are named SSC. In Fig. 1, the region of SSC is depicted. The creep zone size is small in comparison to the crack length and pertinent dimensions of the body and the crack tip is assumed to remain stationary [21].

$W^*$	strain energy rate density
$\delta$	elongation at break
$\phi$	material constant
$\nu$	Poisson’s ratio
$\rho^*$	length of crack extension
$\Gamma$	C-integral path
$\sigma_{ij}$	stress tensor
$\dot{\epsilon}_{ij}$	strain rate
$\dot{\epsilon}_{ss}$	steady-state strain rate
$\epsilon_f^*$	multiaxial creep ductility
$\epsilon_f$	uniaxial creep failure strain
$\hat{\epsilon}_{ij}$	components of strain tensor
$\sigma$	applied stress
$\sigma_{ep}$	stress at 0.05 plastic strain
$\hat{\sigma}_{ij}$	components of stress tensor
$\sigma_f$	fatigue strength coefficient
$\sigma_{ys}$	yield strength
$\sigma_{ult}$	ultimate strength
$\epsilon_f^*$	fatigue ductility coefficient
$\omega_{interaction}$	Lagneborg’s term
$\theta$	polar coordinate of HRR field
$\psi_{y,1}$	UniGrow model constant
$\Delta\kappa$	UniGrow driving force
$\Delta K$	stress intensity factor range
$\Delta K_{th}$	threshold value of $\Delta K$
$\Delta K_{tot}$	total stress intensity factor range
$\Delta\sqrt{J}$	energy release rate factor range

Bassani and McClintock [22] recognized that the crack tip stress fields under SSC can also be characterized by a time-dependent C-integral, whose value is determined along a contour taken very close to the crack tip:

$$C(t) = \int_{\Gamma=0} W^* dy - T_i \frac{\partial u_i}{\partial x} ds \quad (1)$$

where,  $\Gamma$  is a line contour taken counter clockwise from the lower crack surface to the upper crack surface.  $W^*$  is the strain energy rate density (or stress power) associated with the point stress,  $\sigma_{ij}$ , and strain rate,  $\dot{\epsilon}_{ij}$ .  $T_i$  is the component of the traction vector defined by the outward normal,  $n_j$ , along  $\Gamma$  and then,  $T_i = \sigma_{ij} n_j$ . The component of the displacement vector is noted by  $u_i$  and  $ds$  is the arc length along the contour.

$C(t)$  is the same as  $C^*$  but its value is determined close to the crack tip within a region where the creep strains dominate the elastic strains. Thus, close to the crack tip within a region where the creep strains dominate the elastic strains, the  $C(t)$  integral value could be determined along any contour which originated at the lower crack surface, ended on the upper crack surface, and enclosed the crack tip. Hence, determining the  $C(t)$  integral requires accurate solutions of stress and strain near the crack tip. Bassani and McClintock [22] further related the value of  $C(t)$  with the HRR-type stress fields as follows:

$$\sigma_{ij} = \left( \frac{C(t)}{A' I_m r} \right)^{1/(m+1)} \hat{\sigma}_{ij}(\theta, m) \quad (2)$$

$$\dot{\epsilon}_{ij} = A' \left( \frac{C(t)}{A' I_m r} \right)^{m/(m+1)} \hat{\epsilon}_{ij}(\theta, m) \quad (3)$$

where  $A'$ , is the Norton creep constant and,  $m$ , is the Norton creep exponent,  $I_m$  is a constant and  $r$  is the distance from the crack tip. Comparing these equations with the crack tip stress equations in case of SSY [21], we get for the conditions of SSC,

$$C(t) = \frac{[(K^2)(1 - \nu^2)]}{[E(m + 1)t]} \quad (4)$$

where  $t$  is the time. Eq. (4) has been verified by numerical analysis and has been shown [8,9] to be accurate. The  $C(t)$ -integral, because of its ability to characterize the HRR fields from SSC to extensive steady-state creep, is an attractive parameter for correlating creep crack growth rate data. The calculated value is sensitive to the accuracy of the creep constants,  $A'$  and  $m$ , the assumptions regarding the state of stress, and whether primary creep is important. This makes it less desirable for correlating creep crack growth rates.

$$C(t) = \frac{[(K_{max}^2)(1 - \nu^2)]}{[E(m + 1)h_t]} \quad (5)$$

where  $h_t$  is the hold time.

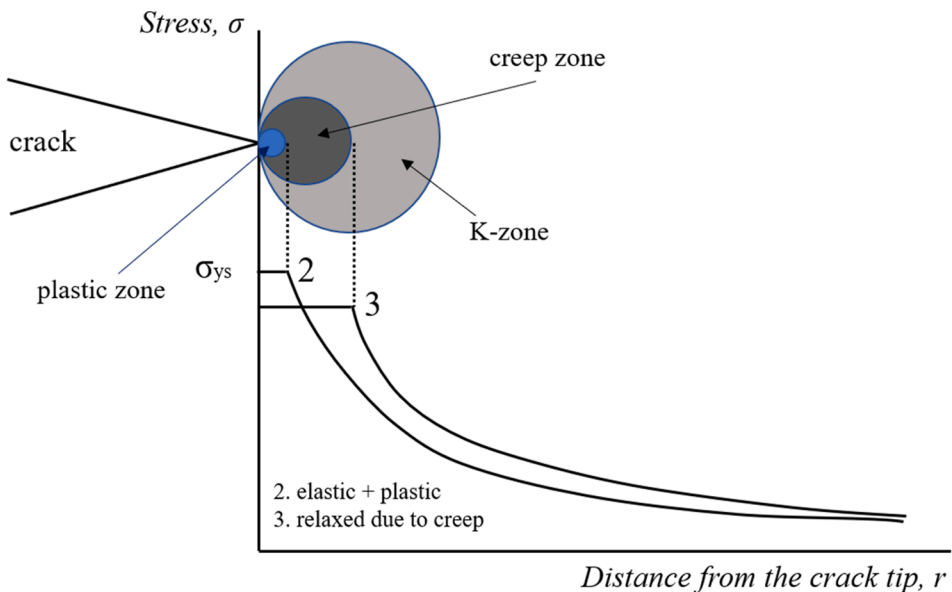


Fig. 1. Region of the SSC.

### 3. A model for creep-fatigue crack propagation and creep-fatigue interaction

A model of creep fatigue damage can be expressed in the following form [13],

$$\left(\frac{da}{dN}\right)_{total} = \left(\frac{da}{dN}\right)_{cycle} + \left(\frac{da}{dN}\right)_{time} \quad (6)$$

The total crack growth per cycle is contributed by the cyclic dependent component and the time dependent component which can be expressed as a linear summation.

It has been widely demonstrated that for a steel alloy such as P91 at high temperature and with hold time equal to 0, the main contribution to the propagation of the crack is linked to cyclical fatigue while, for hold times other than zero, the creep phenomenon contributes more to the crack growth rate compared to fatigue contribution. This increase in the crack growth rate depends on the frequency of the loading cycle which in turn depends on the value of the holding time. It has also been widely demonstrated that, for P91 steel, with a loading cycle frequency greater than 0.0017 Hz [33], the crack propagation is transgranular type while for a frequency equal to or less than 0.0017 Hz, the crack propagation is the intergranular type. In both cases the crack growth rate undergoes an acceleration accompanied by a higher state of constraint.

#### 3.1. Fatigue crack growth law

The unified two-parameter fatigue crack growth driving force model (UniGrow) [34,35] considers the residual stress owing to the application of a cycle load and, subsequently, the stress ratio effect on the fatigue crack growth. The driving force,  $\Delta\kappa$ , is expressed as a combination of the maximum SIF,  $K_{max}$ , and the stress intensity factor range,  $\Delta K$ , corrected for the residual stresses. In its more general formulation that considers the mean stress or the stress ratio effect on fatigue crack propagation, the deformation at the crack-tip material is considered as predominantly plastic. In this work, the UniGrow model has been written with some modifications and introduced inside Zencrack through a FORTRAN user routine during the simulation, similar to the previous nonlinear cases [29,30]. Using the solution provided by Huffman [36],  $K_{max,tot}$  and  $\Delta K_{tot}$  have been calculated with Eq. (7) that, for positive stress ratio, have included residual stresses:

$$K_{max,tot} = K_{max} \left\{ 1 - \left[ \frac{(\sigma_{ep=0.05} - \sigma_{ys})}{\sigma_{ep=0.05}} \right] (1 - R) \right\} \quad (7)$$

where  $\sigma_{ep=0.05}$  is the stress at 0.05 plastic strain,  $\sigma_{ys}$  is the yield strength, and  $R = 0.1$  is the stress ratio imposed with the remote load. It is noteworthy that the  $K_{max}$  introduced in the UniGrow model originates from the fracture mechanics tool calculation of the ERR and is subsequently converted to  $K_{max}$  using the known R-ratio. In other words, in SSY conditions, a conversion factor,  $f_{conv}$ , expressed with equation (8) must be used for calculating  $\Delta K$  from the ERR, expressed in term of  $\Delta\sqrt{J}$ . Thus,

$$f_{conv} = \sqrt{E/(1 - \nu^2)} \quad (8)$$

The resulting equation is as follows:

$$\Delta K = \Delta\sqrt{J} \cdot f_{conv} \quad (9)$$

Subsequently,  $K_{max,tot}$  is calculated using Eq. (7), and  $K_{min,tot} = K_{min}$  because the minimum SIF is unaffected by the residual stresses and is thus equal to the applied  $K_{min}$ . Therefore,  $\Delta K_{tot}$  is calculated using  $K_{max,tot}$  and  $K_{min}$ . Subsequently, starting from the Paris law, the UniGrow model can be written as follows:

$$\left(\frac{da}{dN}\right)_{cyclic} = C' (\Delta\kappa)^\gamma \quad (10)$$

where,  $\gamma = -1/b$

$$\Delta\kappa = \left( K_{max,tot}^p \Delta K_{tot}^{0.5} \right) \quad (11)$$

with,  $p = \frac{n}{(n+1)}$ ,

$$\text{Further, } C' = 2 \rho^* \left\{ \frac{1}{2(\sigma_f')^2} \left[ \left( \frac{\psi_{y,1}}{\sqrt{2\pi\rho^*}} \right)^{3n'+1} \left( \frac{K'}{E^n} \right)^{\frac{1}{n'+1}} \right]^{\frac{1}{2b}} \right\} \quad (12)$$

where,  $K' = \frac{\sigma_f'}{(\sigma_f')^n}$  is the cyclic strength coefficient.

Thus, the crack growth rate can be expressed in the following form:

$$\left(\frac{da}{dN}\right)_{cyclic} = 2\rho^* \left\{ \frac{1}{2(\sigma_f)^2} \left[ \left( \frac{\psi_{y,1}}{\sqrt{2\pi\rho^*}} \right)^{3n+1} \left( \frac{K'}{E^n} \right) \right]^{\frac{1}{(n+1)}} \right\}^{\frac{1}{2b}} \left( K_{max,tot}^p \Delta K_{tot}^{0.5} \right)^{\gamma} \quad (13)$$

Where,  $\rho^*$ , can be written with the following equation:

$$\rho^* = \frac{\pi}{24} (\Delta K_{tot} / \sigma_{ys})^2 \quad (14)$$

where,  $\rho^*$  is the radius of the cyclic plastic zone,  $\sigma_{ys}$  is the yield strength of the material, and  $\Delta K_{tot}$  is obtained as the difference between  $K_{max,tot}$  and  $K_{min}$ , as previously described. Eq. (15) resembles the plastic zone size correction proposed by Edmunds and Willis [37] in which, instead of  $K_I$ ,  $\Delta K_{tot}$  is used. Furthermore, in Eq. (14),  $\sigma_{ys}$  is used instead of cyclic  $\sigma_{ys}$  because  $\Delta K_{tot}$  in the modified version of UniGrow model is expressed as function of R-ratio that depends on the monotonic load. Finally, it is noteworthy that the fatigue crack propagation law (13) is written using the Manson-Coffin equation, in which the plastic term is omitted [34]. Additionally, it should be noted that the driving force (11) results directly from the mean stress correction model, i.e. the Smith, Watson, and Topper fatigue damage parameter [34].

### 3.2. Time dependent crack growth law

For a C(T) specimen the crack growth rate (CGR) and  $C^*$  integral under steady state condition can be represented as  $da/dt = DC^{*\phi}$  where D and  $C^*$  are the creep crack growth (CCG) power-law coefficient and exponent respectively [33] and  $\phi$  is a material constant, generally equal to 0.85 [33]. Then, the CCG rate can be estimated using the NSWA approximate crack growth model proposed by Nikbin et al. [33] reported in that follows,

$$\left(\frac{da}{dt}\right)_{NSWA} = DC^{*0.85} \quad (15)$$

where,  $D = 3/\varepsilon_f^*$  and  $\varepsilon_f^*$  is the multiaxial creep ductility, which is usually taken as uniaxial creep failure strain,  $\varepsilon_f$  for plane stress condition and  $\varepsilon_f/30$  for plane strain condition [33]. Hence,

$$\left(\frac{da}{dt}\right)_{NSWA} = \frac{3C^{*0.85}}{\varepsilon_f} \quad (16)$$

In SSC conditions,  $C^*$  is equivalent to C(t) integral [21] thus,

$$\left(\frac{da}{dN}\right)_{time} = D[(C(t)^{0.85})] h_t \quad (17)$$

where,  $h_t$  [h] is the hold time.

### 3.3. Creep-fatigue interaction

Under conditions of both SSY and SSC, the crack propagation can be assumed as the linear sum of fatigue and creep crack growth rates [13]. Lagneborg in [14] identifies the effect of the low-cycle fatigue and creep combination on the life of stainless steels and established a term,  $\omega_{interaction}$ , to describe the damage due to the creep-fatigue interaction reported in that follows,

$$\omega_{interaction} = b_i \left[ \left(\frac{da}{dN}\right)_{cycle} \left(\frac{da}{dN}\right)_{time} \right]^{0.5} \quad (18)$$

where,  $b_i$  is a creep-fatigue interaction coefficient. According to the experimental data of creep-fatigue shown in [1] for the P91 steel at 625 °C,  $b_i = 3.25$  for a holding time,  $t_h = 600$  s, while  $b_i = 4.45$  for a holding time  $t_h = 60$  s. In [13] it has been also described that the term,  $b_i$ , can be indicated as  $b_i = 7.78 \times t_h^{0.1365}$ . Thus, the equation (6) can be rewritten as,

$$\left(\frac{da}{dN}\right)_{total} = \left(\frac{da}{dN}\right)_{cycle} + \left(\frac{da}{dN}\right)_{time} + b \left[ \left(\frac{da}{dN}\right)_{cycle} \left(\frac{da}{dN}\right)_{time} \right]^{0.5} \quad (19)$$

where, the first term on the right-hand side, is related to the contribution of the fatigue component, the second is related to creep (time dependent) process, while the third is due to the creep-fatigue interaction. Recently, the creep-fatigue damage term proposed by Lagneborg [14] has been reconsidered by Jing et al. [13] and it has been adopted in this work. Then, in this case of study, since a frequency of about 0.0017 Hz occurs at a hold time  $t_h = 60$  s, the  $\omega_{interaction}$  has been considered negligible in the equation (19), while on the contrary, this term is not negligible for a holding time,  $t_h = 600$  s, because of creep-fatigue interaction that significantly increases the crack growth rate [13]. Thus, in a general form, the final crack growth rate law can be expressed as reported in that follows,

$$\left(\frac{da}{dN}\right)_{total} = [C' \Delta \kappa^r]_{cyclic} + \{D[(C(t)^{0.85})]h_t\}_{time} + b\{[C \Delta \kappa^r][D(C(t)^{0.85})h_t]\}^{0.5} \quad (20)$$

#### 4. Materials and methods

Since the determination of the J-integral, in finite element codes (FE), is based on the domain integral method in contour integral evaluation, which was initially suggested by Parks [23,24] and further developed by DeLorenzi [25,26] and the domain integral is based on the amount of energy applied to a finite region of elements, this method is considerably robust and precise values can also be obtained using relatively coarse meshes. Since the J-integral is also defined in terms of ERR associated with a fictitious advancement of small cracks, the domain integral method is also known as the “virtual crack extension” method [18] (VCE).

The commercial software for damage tolerance simulations Zencrack [27], has been used to simulate crack propagation. Zencrack works with contour integral evaluation and the VCE method. Thus, to make the fatigue calculation, it is not necessary to apply a cyclic remote load but only a static load up to its maximum value. Furthermore, in constant amplitude loading, the R-ratio is used for calculating the minimum SIF and then  $\Delta K$ . With this approach, the unloading of the specimen never occurs, and the material behaviour is nonlinear making the transition creep (TC) condition negligible.

Then, Abaqus [28] and Zencrack software interact each other in such a way the crack fatigue propagation is obtained by means of a series of incremental steps in which the maximum value of the applied remote load is reached while the number of cycles is calculated by means of the fatigue law introduced in the fracture mechanics tool with an external FORTRAN routine. Furthermore, considering the SSY conditions, the crack is modelled in such a way that the root of the crack front can proportionally blunt with applied load. Hence, the use of the VCE allows to carry out the crack insertion through incremental steps. The crack growth simulations are carried out using the modified UniGrow model [20,29,30] considering a nonlinear behaviour for the material under both the SSY and SSC conditions.

Then, the material behaviour of P91 steel is modelled accordingly to the Ramberg-Osgood equation through the true stress-strain curve shown in Fig. 2, where  $n > 10$  is the strain hardening exponent that indicates an ideal plasticity condition [16], where,  $E$ , is the Young's modulus,  $\sigma_{ys}$ , is the tensile yielding strength,  $\sigma_{ult}$ , is the ultimate strength of the material and,  $\delta$ , is the elongation at break.

In Table 1, the material properties of P91 steel at 625 °C have been reported [1].

Since the P91 steel is an elastic power-law creeping material subjected to a temperature of 625 °C, in the secondary creep regime, the minimum creep rate has been linearly fit using Norton's power law,  $\dot{\epsilon}_{ss} = A' \sigma^m$ , where  $\dot{\epsilon}_{ss}$  is the steady-state strain rate and  $\sigma$  is the applied stress. In Table 2, the constants of steel P91 in creep conditions are shown.

For assessing the micro structural damage that occurs within the plastic zone ahead of the crack front, LCF properties must be considered [19,20,29,30]. Such properties for the P91 steel (Table 3) have been found in the literature for a temperature of 625 °C [1]. Since in the literature the data available on the properties of LCF are not unique, these properties have been calibrated on the basis of the available experimental data and subsequently introduced in the modified UniGrow law for fatigue crack propagation through a special FORTRAN user routine in Zencrack [27]. Table 3, has been reported in that follows,

where,  $\Delta K_{th}$  is threshold of  $\Delta K$ ,  $b$  is the fatigue strength exponent;  $c$  is the fatigue ductility exponent;  $\sigma'_f$ , is the fatigue strength coefficient and,  $\epsilon'_f$ , is the fatigue ductility coefficient;  $n'$ , is the cyclic strain hardening exponent.

#### 5. Experimental data

Experimental tests on C(T) specimens at elevated temperature of 625 °C and creep-fatigue tests have been carried out by Narasimhachary and Saxena [1]. Then, creep rupture tests have been performed under uniaxial, constant force and controlled temperature

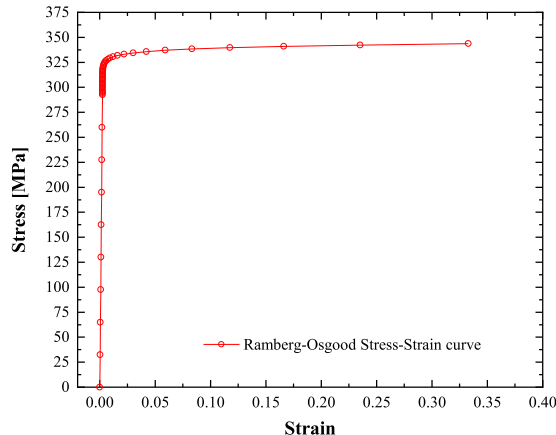


Fig. 2. Ramberg-Osgood stress-strain curve for P91 steel at 625 °C.

**Table 1**  
Material properties of P91 steel at 625 °C.

E (MPa)	$\nu$	$\sigma_{ys}$ (MPa)	$\sigma_{ult}$ (MPa)	$\delta$ (%)
125,000	0.3	325	347	33

**Table 2**  
Creep constants of P91 steel at 625 °C.

A' (MPa) <sup>n</sup> h <sup>-1</sup>	m
3.25e-22	8.24

**Table 3**  
Threshold of  $\Delta K$  and LCF properties for the P91 steel at 625 °C.

$\Delta K_{th}$ (MPa mm <sup>0.5</sup> )	$\sigma_f$ (MPa)	$\epsilon_f'$	$n'$	b	c
253	400	1.171	0.19	-0.068	-0.357

of 625 °C in a lab-controlled atmosphere, as required per ASTM E139 [31]. The C(T) specimens have been pre-cracked to an initial crack length to width ratio,  $a/W$ , of about 0.4, under cyclic loading at room temperature. To produce a uniform crack growth, all specimens have been side grooved by 10% of the specimen thickness on each side. The crack front in C(T) specimen without side grooves display an arched shape known as crack tunnelling. During its propagation, the crack front tends to assume this curvature due to varying levels of plastic constraint across specimen thickness [40]. Side grooves are recommended by ASTM E 1457-00 [41] to ensure that a straight crack front is produced.

Then, the experimental tests have been conducted in both electric-actuator and servo-hydraulic test machines in Westmoreland (W) and BISS (B) Laboratories with hold times of 0 s, 60 s and 600 s, respectively and the results, available in the literature [1], have been reported in Table 4.

It is worth noting that, for a zero-hold time only fatigue has been estimated. Waveforms for loading and unloading portions are triangular while the loading rates are constant (see Fig. 3).

In Fig. 3, hold times of predetermined duration, 2 s, have been superimposed on the triangular waveforms at maximum load [13]. All tests have been carried out using a R-ratio of 0.1.

## 6. Geometry, loads and boundary conditions of the numerical model

C(T) specimen geometry and dimensions have been chosen according to the ASTM for test standard [32]. Dimension of C(T) specimen has been reported in Fig. 4.

Load and boundary conditions have been applied on the numerical model of the C(T) specimen in order to reproduce the experimental test conditions. Furthermore, load and boundary conditions have been applied by means of two reference points, RP<sub>1</sub> and RP<sub>2</sub> (see Fig. 5). Constraints have been applied in the global reference system to prevent displacements  $u_1$  and  $u_3$ . Displacement  $u_2$  has been allowed. Rotations, rotX, around the X axis and, rotY, around the Y axis have been prevented. Rotation, rotZ, around the Z axis has been allowed (see Fig. 5).

To reproduce the test conditions, an environmental temperature of 625 °C has been also applied.

To perform simulations of several experimental tests, different values of the external load and hold time have been applied to the C(T) specimen model. It is worth noting that, structural distributing conditions [28] have been used to couple the load with half hole surfaces as shown in Fig. 5 (red colour). The crack propagation has been simulated under displacement control and the stress relaxation due to the creep phenomenon has been allowed introducing a hold time. The numerical model of the C(T) specimen has been grooved with an angle of 120° to prevent possible remeshing issues of the crack front during its propagation.

**Table 4**  
Test conditions for C(T) specimens under FCG and CFCG conditions.

Specimen ID	Hold time (s)	Max Load (kN)	Initial $\Delta K$ (MPa*m <sup>0.5</sup> )	Final $\Delta K$ (MPa*m <sup>0.5</sup> )	Crack length Initial (mm)	Crack length Final (mm)	Cycles N <sub>f</sub>
3-1-1(W)	0	9.0	23.9	57.5	20.25	33.06	15,790
3-1-2(W)	60	9.0	23.6	39.51	19.90	28.50	3470
3-1-3(W)	600	9.0	23.9	35.6	20.27	27.00	763
3-1-4(W)	60	7.5	19.6	38.9	19.92	30.70	8018
3-1-5(W)	600	7.5	19.6	29.5	19.95	26.90	1915
3-1-8(B)	0	9.0	23.0	53.0	19.54	32.17	16,298
3-1-9(B)	0	11.0	29.1	56.7	20.17	30.59	8800

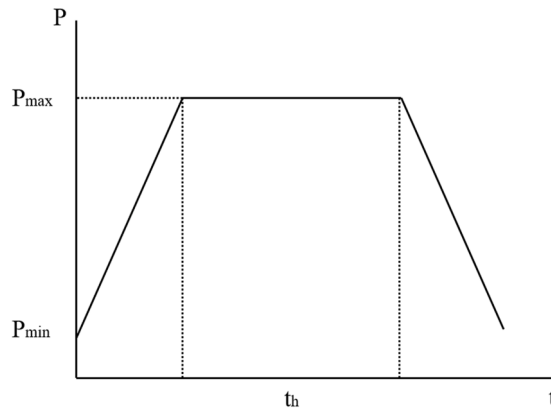


Fig. 3. The diagram of cyclic loading.

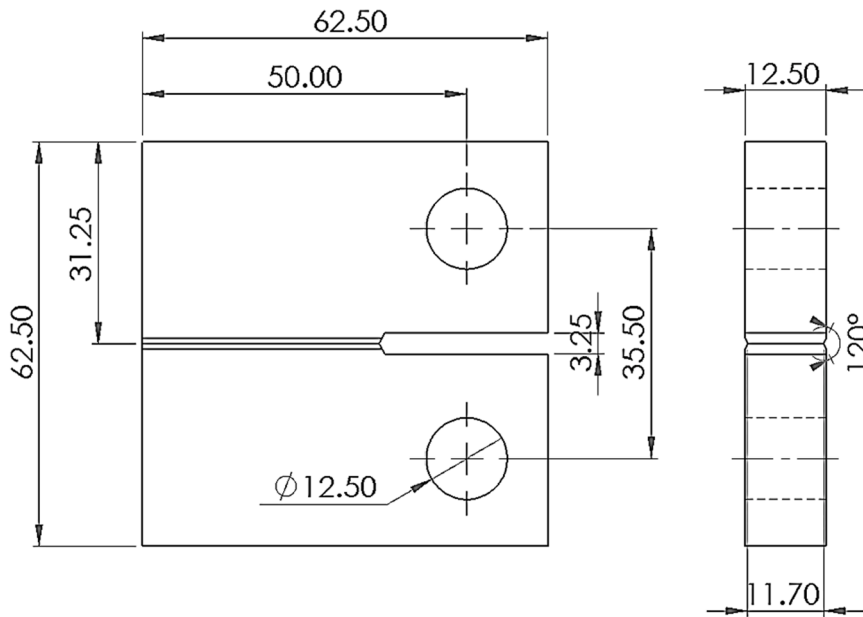


Fig. 4. Geometry and dimensions of the numerical model (mm).

## 7. Results and discussion

An initial notch,  $a_0 = 13.5$  mm, has been introduced in the FE model. The FE model has been meshed with 72,044 8-noded linear brick elements (C3D8). The points A, B, C, positioned along the crack front (see Fig. 6), have been used for measuring the crack's advancement during the propagation. Hence, the C point has been positioned at the middle of the crack front, whilst the measuring points, A, B, were obtained to the intersection of the crack front with the free surfaces of the specimen. Then, several load cases have been reported and the numerical and experimental results have been compared each other in Tables 5-7.

### 7.1. 9.0 kN load case – Fatigue, creep (hold times 60 s and 600 s)

For a hold time equal to zero seconds, that is, if the only fatigue has been considered, the load case has been made up one only step (ID 3-1-1(W)). Instead, for a hold time different from zero seconds the load case has been split in two steps (step1 and step2). Furthermore, a uniform environmental temperature of 625 °C and a remote tensile load been applied. The load has been statically applied up to its maximum value. In Fig. 7, the FE meshed model of the loaded C(T) specimen has been shown and the von Mises stress solutions at the crack tip, related to the hold time = 0 s and the hold times equal to 60 s (ID 3-1-2(W)) and 600 s (ID 3-1-3(W)), respectively, have been highlighted.

In Fig. 8a, the von Mises stress distribution have been shown with highlighting of the crack front at the start of the crack

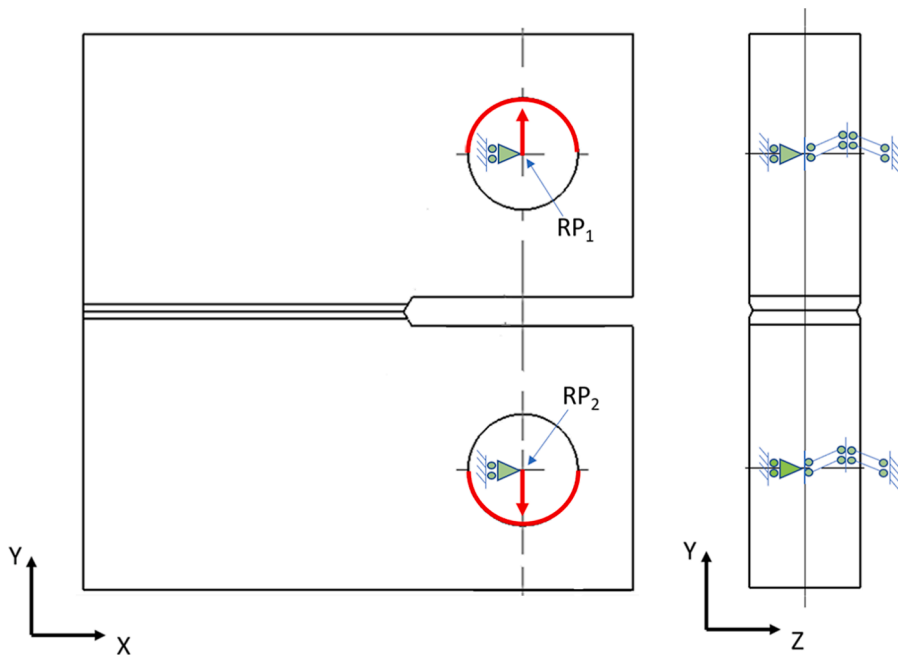


Fig. 5. Load and boundary conditions applied on the reference points  $RP_1$  and  $RP_2$ , respectively.

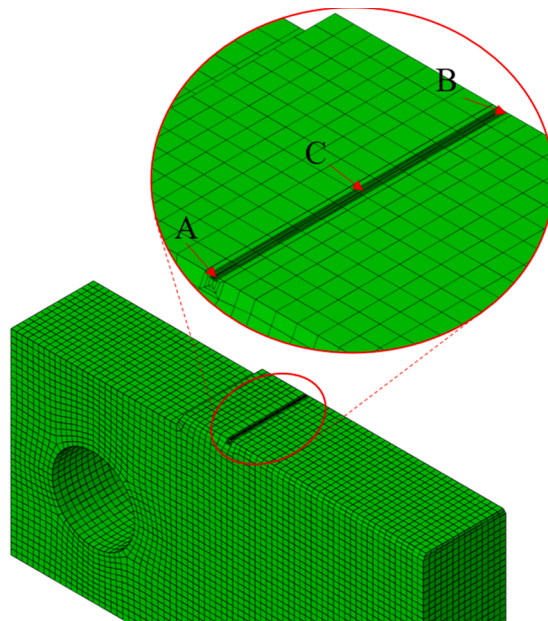


Fig. 6. The C(T) model with highlighting of the measuring points A,B,C along the crack front.

**Table 5**

Comparison between numerical and experimental results with hold time = 0 s.

Specimen ID	Hold time (s)	Max Load (kN)	Initial $\Delta K$ ( $MPa \cdot m^{0.5}$ )	Final $\Delta K$ ( $MPa \cdot m^{0.5}$ )	Crack length Initial (mm)	Crack length Final (mm)	Cycles $N_f$
<i>Experimental</i>	0	9.0	23.9	57.5	20.25	33.06	15,790
<i>Numerical</i>	0	9.0	23.89	57.77	20.25	33.3	15,825

**Table 6**

Comparison between numerical and experimental results with hold time = 60 s.

Specimen ID	Hold time (s)	Max Load (kN)	Initial $\Delta K$ (MPa $\cdot$ m <sup>0.5</sup> )	Final $\Delta K$ (MPa $\cdot$ m <sup>0.5</sup> )	Crack length Initial (mm)	Crack length Final (mm)	Cycles $N_f$
<i>Experimental</i>	60	9.0	23.6	39.51	19.9	28.5	3470
<i>Numerical</i>	60	9.0	23.52	39.84	19.9	28.42	3455

**Table 7**

Comparison between numerical and experimental results with hold time = 600 s.

Specimen ID	Hold time (s)	Max Load (kN)	Initial $\Delta K$ (MPa $\cdot$ m <sup>0.5</sup> )	Final $\Delta K$ (MPa $\cdot$ m <sup>0.5</sup> )	Crack length Initial (mm)	Crack length Final (mm)	Cycles $N_f$
<i>Experimental</i>	600	9.0	23.9	35.6	20.27	27	763
<i>Numerical</i>	600	9.0	23.52	38.26	20.25	26.71	702

propagation and for the case with hold time equal to zero seconds (only fatigue). The region ahead of the crack front and interested by plasticity is very small compared to the other specimen sizes so that the SSY conditions can be satisfied. In Fig. 8b,c, it is possible to observe different amount of stress relaxation due to the creep conditions for a hold time of 60 s (a) and 600 s (b), respectively.

In Fig. 9a, the von Mises stress distribution have been shown with highlighting of the crack front at the final step of the crack propagation and for the case with hold time equal to zero seconds (only fatigue). The region ahead of the crack front and interested by plasticity is quite large compared to the other specimen sizes so that the SSY conditions cannot be satisfied. In Fig. 9b,c, it can be observed the huge amount of stress relaxation due to the creep conditions for a hold time of 60 s (a) and 600 s (b), respectively.

As expected, the crack propagated inside the material and the measuring point C has grown quicker than the other points, A and B, respectively. This effect has been more evident considering the only fatigue (hold time = 0 s) because of the higher triaxiality stress in the region close to the centre of the crack front and this because of the lower constraint relaxation. On the contrary, when the creep phenomenon has been considered, the stress relaxation in the cracked region have produced lower triaxiality stress in the region close to the centre of the crack front and then a higher constraint relaxation. Furthermore, there was no evidence of extension creep (EC).

### 7.2. 9.0 kN – fatigue

In Table 5, a comparison between the numerical and experimental results has been shown. The experimental data reported in Table 5 comes from Table 4 for a hold time = 0 s. Modelling the initial crack with the same size of the experimental test, a good agreement between the values has been found at the end of the simulation of crack propagation. In this case there was a minimal difference of 0.2%.

In Fig. 10, the crack lengths measured in the points A, B and C versus the number of cycles, have been reported showing an elliptical similar form at the end of the crack propagation.

### 7.3. 9.0 kN – Fatigue and creep (hold time 60 s)

In Table 6, a comparison between the numerical and experimental results has been shown for a hold time = 60 s (fatigue and creep). Modelling the initial crack with the same size of the experimental test, a good agreement between the values has been found at the end of the simulation of crack propagation. In this case there was a minimal difference of 0.4%.

In Fig. 11, the crack lengths measured in the measuring points A, B and C versus the number of cycles, have been reported showing an elliptical similar form at the end of the crack propagation less pronounced than for the case with hold time = 0 s. This behaviour has been due to a more uniform distribution of the constraint relaxation along the central part of the crack front. Furthermore, it is worth noting that final number of cycles shown in Fig. 11 has been numerically obtained by a linear sum of creep (time dependent) and fatigue crack growth rates as described previously in Eq. (20).

### 7.4. 9.0 kN – Fatigue, creep (hold time 600 s) and Creep-Fatigue interaction

In Table 7, a comparison between the numerical and experimental results has been shown for a hold time = 600 s when fatigue, creep and creep-fatigue interaction have been experimentally observed [33]. Adopting all terms described on the right side of the Eq. (20), namely considering also the term related to creep-fatigue interaction proposed by Lagneborg [14], a good agreement between the values has been found at the end of the crack propagation simulation.

In this case there was a greater difference of 8% between the data respect to the previous cases with hold times 0 s and 60 s. In the latter case it should be noted that the numerical final crack advancement has been less than 0.29 mm than the experimental one. In Fig. 12, the crack lengths measured in the measuring points A, B and C versus the number of cycles have been reported, showing an elliptical similar form at the end of the crack propagation less pronounced than for the cases with hold time = 60 s and hold time = 0 s. The final number of cycles shown in Fig. 12b has been numerically obtained by a linear sum of fatigue, creep (time dependent) and creep-fatigue interaction crack growth rates.

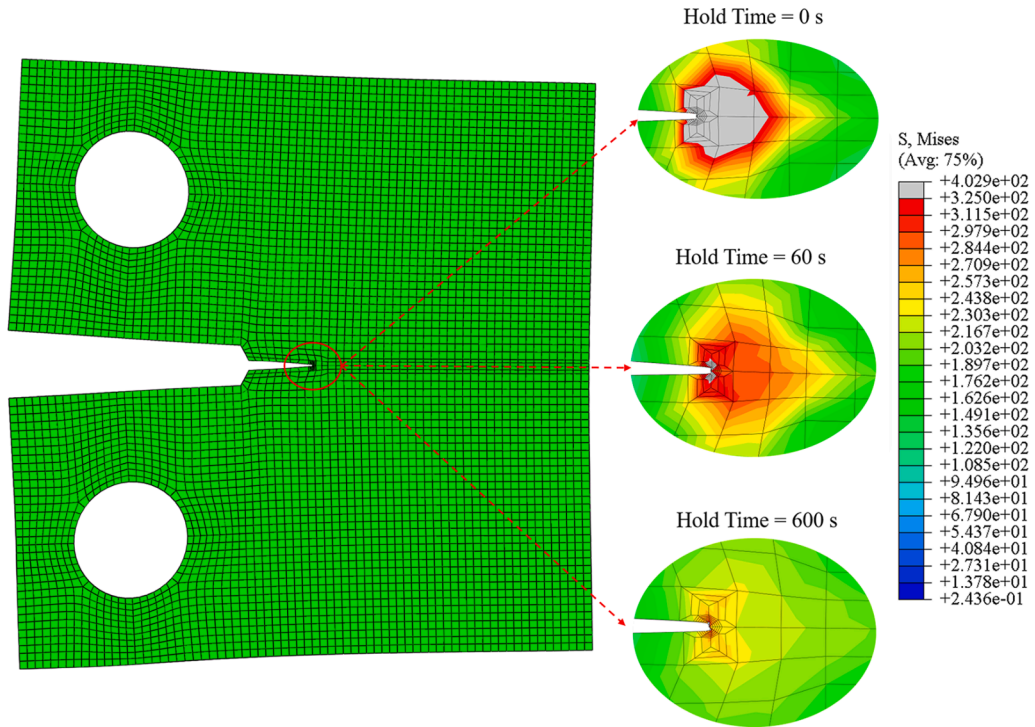


Fig. 7. FE model corresponding to its configuration of maximum tensile load (left) and the von Mises stress distribution (MPa) in the cracked region highlighted (right) for different values of the hold times (0 s, 60 s and 600 s).

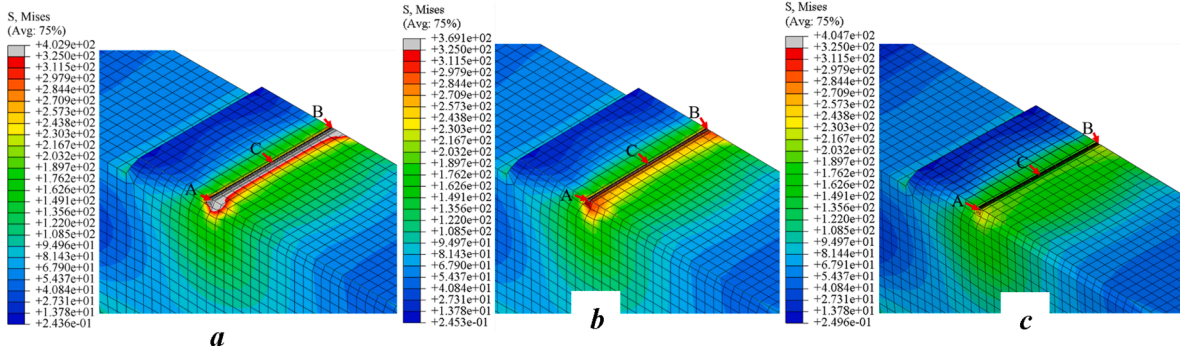


Fig. 8. a,b,c. Distribution of von Mises stresses (MPa) along the initial crack front with highlighting of the cracked region for hold time = 0 s (a), hold time = 60 s (b) and hold time = 600 s (c).

### 7.5. Other results

In Fig. 13a,b, the crack lengths corresponding to the measuring points A, B and C of the crack front and related to the 7.5 kN load case and specimens ID 3-1-4(W) and ID 3-1-5(W), respectively, have been shown. According to the experimental results, a satisfactory agreement has been found. In these cases, the level of constraint ahead of the crack front is lower than the 9.0 kN load case, indicating that the crack shape is dependent by the remote load applied.

In Fig. 14a, the crack lengths corresponding to the points A, B and C of the crack front and related to the 9.0 kN (ID 3-1-8(B)) load case has been shown. In Fig. 14b, the crack lengths corresponding to the points A, B and C of the crack front and related to the 11.0 kN (ID 3-1-9(B)) load case has been shown.

For sake of brevity, all results and relative comparisons have been reported schematically in Table 8. In this table, numerical and experimental results have been reported as well as the ID of the specimens.

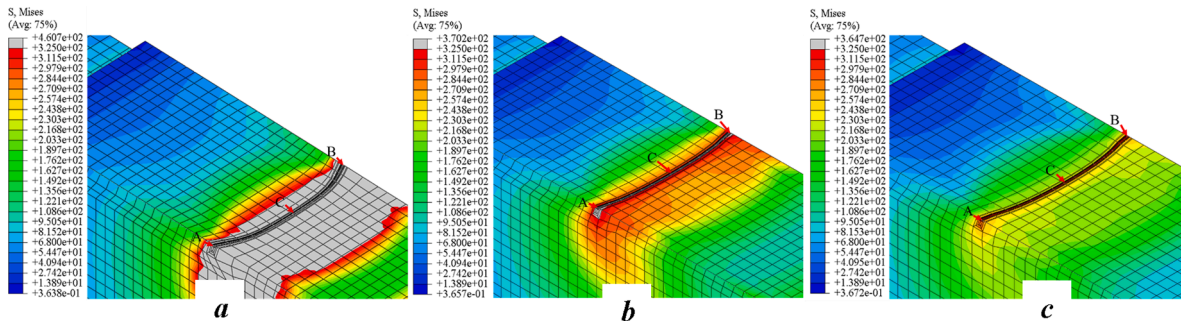


**Fig. 9.** a,b,c. Distribution of von Mises stresses (MPa) along the final crack front with highlighting of the cracked region for hold time = 0 s (a), hold time = 60 s (b) and hold time = 600 s (c).

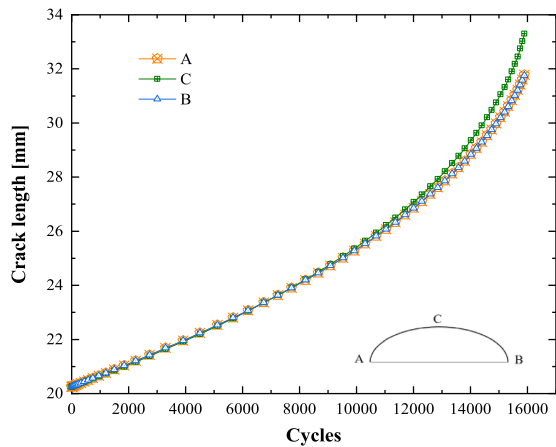


**Fig. 10.** Comparison between the crack lengths measured in the points A, B and C versus the number of cycles for hold time = 0 s.

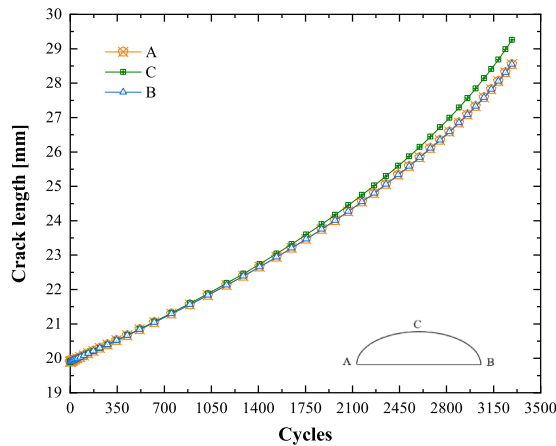


**Fig. 11.** Comparison between the crack lengths measured in the points A, B and C versus the number of cycles for hold time = 60 s.

## 8. Conclusions

The experimental tests on P91 steel at high temperature and provided by Narasimhachary and Saxena [1] have been simulated using commercial FE-based software in the SSY and the SSC conditions. Several loading cases and boundary conditions applied on the numerical model of the specimen have been chosen according to the experimental tests. Because of the SSY condition, the nonlinear behaviour of P91 steel has been modelled by means of the Ramberg-Osgood equation and to model the creep behaviour the Norton's power law has been adopted. Hence, the modified UniGrow nonlinear model has been taken into account to carry out the simulations

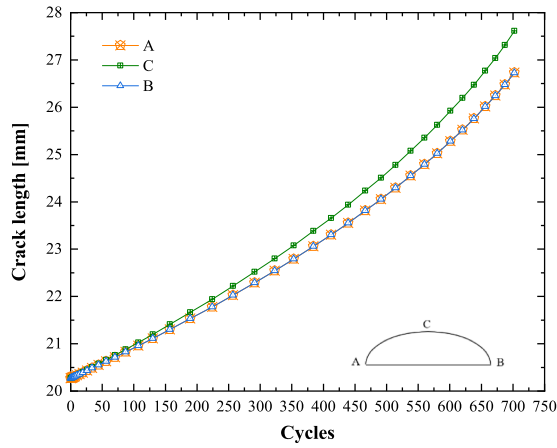


Fig. 12. Comparison between the crack lengths measured in the points A, B and C versus the number of cycles for hold time = 600 s.

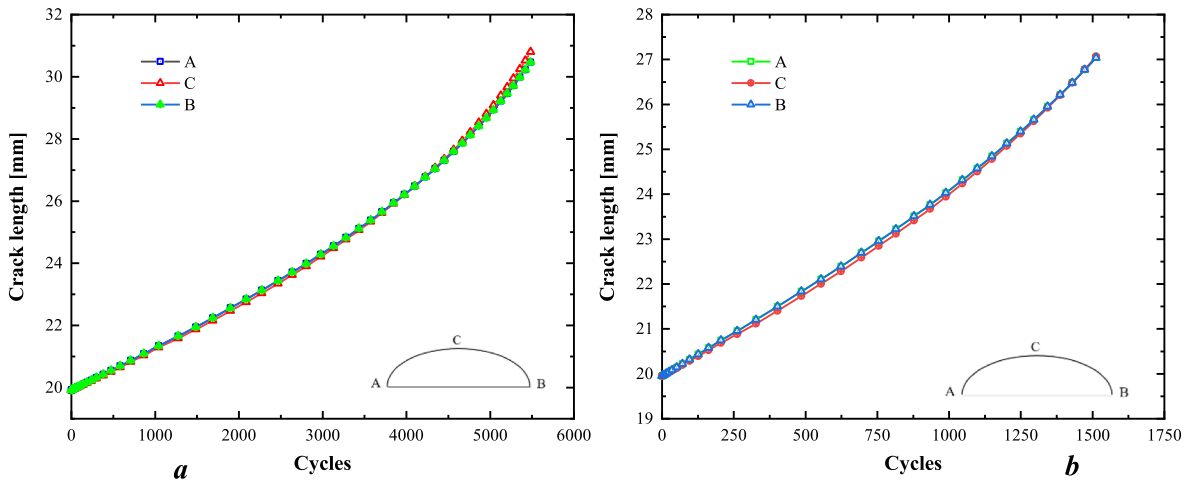


Fig. 13. a,b. 7.5 kN load case with hold time 60 s (a) and 600 s (b).

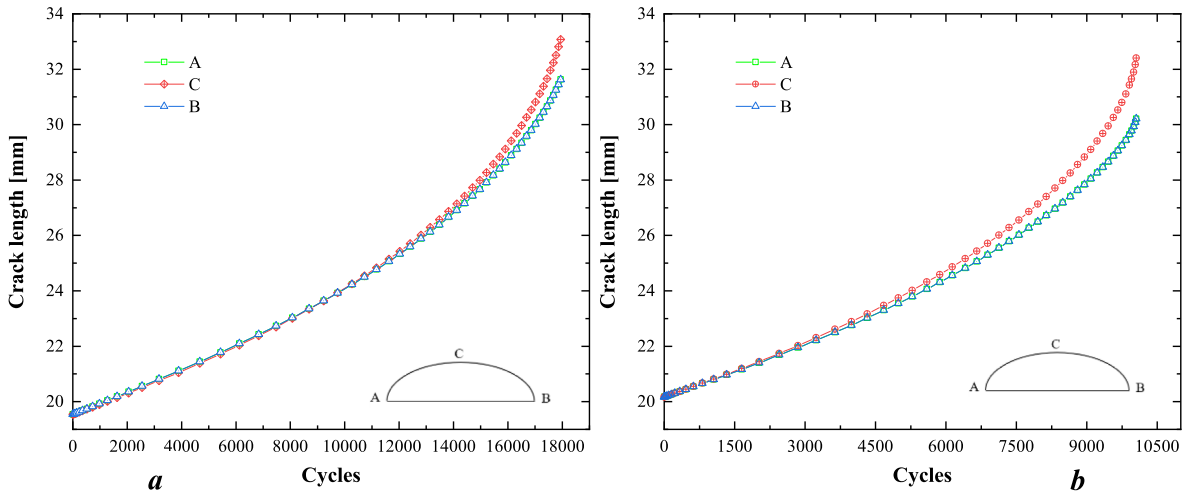


Fig. 14. a,b. Hold time equal to 0 s. 9 kN (B) load case (a), 11 kN (B) load case (b).

**Table 8**

Comparison between experimental and numerical results.

Specimen ID	Test type	Hold time (s)	Max Load (kN)	Initial $\Delta K$ (MPa $\cdot$ m <sup>0.5</sup> )	Final $\Delta K$ (MPa $\cdot$ m <sup>0.5</sup> )	Crack length Initial (mm)	Crack length Final (mm)	Cycles N <sub>f</sub>
3-1-1(W)	FCG	0	9.0	23.9	57.5	20.25	33.06	15790
FEM		0	9.0	23.89	57.77	20.25	33.3	15825
3-1-8(B)	FCG	0	9.0	23.0	53.0	19.54	32.17	16298
FEM		0	9.0	23.08	55.6	19.54	31.63	17944
3-1-9(B)	FCG	0	11.0	29.1	56.7	20.17	30.59	8800
FEM		0	11.0	28.26	82.61	20.17	30.17	10052
3-1-2(W)	FCG and CFCG	60	9.0	23.6	39.51	19.90	28.50	3470
FEM		60	9.0	23.52	39.84	19.90	28.42	3455
3-1-4(W)	FCG	60	7.5	19.6	38.9	19.92	30.70	8018
FEM		60	7.5	20.1	34.09	19.92	30.79	5482
3-1-3(W)	FCG, CFCG and Creep-Fatigue interaction	600	9.0	23.9	35.6	20.27	27.00	763
FEM		600	9.0	23.3	38.26	20.27	26.71	702
3-1-5(W)	FCG	600	7.5	19.6	29.5	19.95	26.90	1915
FEM		600	7.5	20.12	27.58	19.95	27.04	1512

of creep fatigue crack propagation considering also the creep-fatigue interaction using the Lagneborg's term [13]. The crack fronts have been modelled to consider the blunting effect and the load has been applied for all loading cases with a stress ratio, R, equal to 0.1. The FE simulations have been performed considering three different values of the hold time, 0 s, 60 s and 600 s. A comparison between numerical and experimental results has been carried out showing a good agreement. At the crack tip and for a long hold time test such as 600 s, creep deformation and cavitation play an important role in the damage mechanisms compared to shorter hold times. Finally, this numerical approach has clearly shown its advantage as it can be applied to structural components with complex geometry and challenging loading.

The main conclusions produced by this study can be summarized as follows:

- it is possible to model the creep fatigue stress-strain field, ahead of the crack front, of P91 steel by means of the Ramberg-Osgood equation and the Norton's power creep law in SSY and SSC conditions.
- the LCF properties and the C(t) integral have been used to perform the numerical simulations.
- the modified UniGrow model can effectively predict the crack growth rates for creep fatigue and creep-fatigue interaction with use of commercial software.
- for tests with hold time of 0 s, a satisfactory agreement between the numerical and the experimental results has been found.
- for tests with hold time of 60 s, the comparison between the numerical and experimental final number of cycles is satisfactory only if added the time dependent component.
- for the longer hold time tests of 600 s, the numerical and experimental comparison between the final number of cycles is satisfactory only if the Lagneborg creep-fatigue interaction is added to the cyclic and time dependent damage.

## Declaration of Competing Interest

The authors declare that they have no known competing financial interests or personal relationships that could have appeared to influence the work reported in this paper.

## References

- [1] S.B. Narasimhachary, A. Saxena, Crack growth behavior of 9Cr-1Mo (P91) steel under creep-fatigue conditions, *Int. J. Fatigue* 56 (2013) 106–113.
- [2] P.S. Grover, A. Saxena, Developments in creep-fatigue crack growth testing and data analysis, *ECF 10–Struct. Integrity: Exp.–Models–Appl.* 1 (1994) 3–21.
- [3] A. Shibli, F. Starr, Some aspects of plant and research experience in the use of new strength martensitic steel P91, *Int. J. Pres. Ves. Pip.* 84 (2007) 114–122.
- [4] R.W. Swindeman, et al., Issues in replacing Cr-Mo steel and stainless Steels with 9Cr-1Mo-V steel, *Int. J. Pres. Ves. Pip.* 81 (2004) 507–512.
- [5] Y.L. Lu, et al., Effects of temperature and hold time on creep-fatigue crack-growth behavior of HAYNES® 230® alloy, *Mater. Sci. Eng.* 429 (1–2) (2006) 1–10.
- [6] F. Bassi, S. Foletti, A.L. Conte, Creep Fatigue Crack Growth and Fracture Mechanism at T/P91 Power Plant Steel, *Mater. High Temp.* 32 (2015) 250–255.
- [7] S.R. Holdsworth, Creep Fatigue Interaction in Power Plant Steels, *Mater. High Temp.* 28 (2011) 197–204.
- [8] J.F. Wen, S.T. Tu, X.L. Gao, J.N. Reddy, Simulations of creep crack growth in 316 stainless steel using a novel creep-damage model, *Eng. Fract. Mech.* 98 (2013) 169–184.
- [9] L. Zhao, et al., Analysis of creep crack growth behavior of P92 steel welded joint by experiment and numerical simulation, *Mater. Sci. Eng., A* 558 (2012) 119–128.
- [10] T.H. Hyde, M. Saber, W. Sun, Creep crack growth data and prediction for a P91 weld at 650°C, *Int. J. Pres. Ves. Pip.* 87 (12) (2010) 721–729.
- [11] M. Saber, W. Sun, T.H. Hyde, Numerical study of the effects of crack location on creep crack growth in weldment, *Eng. Fract. Mech.* 154 (2016) 72–82.
- [12] S. Taira, Lifetime of structures subjected to varying load and temperature, in: *Creep in structures*, Springer, 1962, pp. 96–124.
- [13] H. Jing, et al., Finite element simulation of creep-fatigue crack growth behavior for P91 steel at 625°C considering creep-fatigue interaction, *Int. J. Fatigue* 98 (2017) 41–52.
- [14] R. Lagneborg, R. Attermo, The effect of combined low-cycle fatigue and creep on the life of austenitic stainless steels, *Metall Trans* 2 (7) (1971) 1821–1827.
- [15] J.W. Hutchinson, Crack-tip singularity fields in non-linear fracture mechanics: a survey of current status, *Adv. Fract. Res.* 6 (1982) 2669–2684.
- [16] M. Kuna, Finite elements in fracture mechanics, *Theory–Numer.–Appl. Solid Mech. Appl.* 201 (2013).

- [17] A.T. Zehnder, *Fracture Mechanics*, Springer, Netherlands, 2012 doi:10.1007/978-94-007-2595-9.
- [18] W. Brocks, *Plasticity and Fracture*, Springer, Netherlands, 2018 doi:10.1007/978-3-319-62752.
- [19] D. Kujawski, F. Ellyin, A fatigue crack growth model with load ratio effects, *Eng. Fract. Mech.* 28 (1987) 367–378.
- [20] M. Lepore, F. Berto, On the fatigue propagation of multiple cracks in friction stir weldments using linear and non-linear models under cyclic tensile loading, *Eng. Fract. Mech.* 206 (2019) 463–484.
- [21] A. Saxena, *Advanced Fracture Mechanics and Structural Integrity*, CRC Press, 2019 doi:10.1201/9781351004060.
- [22] J.L. Bassani, F.L. McClintock, Creep relaxation of stress around a crack tip, *Int. J. Solids Struct.* 17 (1981) 79–89.
- [23] D.M. Parks, A stiffness derivative finite element technique for determination of crack tip stress intensity factors, *Int. J. Fract.* 10 (4) (1974) 487–502.
- [24] D.M. Parks, The virtual crack extension method for non-linear material behaviour, *Comput. Methods Appl. Mech. Eng.* 1 (1977) 353–364.
- [25] H.G. DeLorenzi, Energy release rate calculations by the finite element method, *General Electric Technical Information Series, Report No. 82CRD205*, 1982.
- [26] H.G. DeLorenzi, On the energy release rate and the J-integral for 3D crack configurations, *J. Fract.* 19 (3) (1982) 183–193.
- [27] Zencrack v8.3.1 - 12,2018. Documentation, Zentech International Limited, 2018.
- [28] Dassault Systems, Simulia Corp, Abaqus analysis user's manual, Version 2020, Providence, RI, USA, 2020.
- [29] M. Lepore, et al., Nonlinear fatigue crack propagation in a baffle module of Wendelstein 7-X under cyclic bending loads, *Fatigue Fract. Eng. Mater. Struct.* 1–11 (2019), <https://doi.org/10.1111/ffe.13013>.
- [30] M. Lepore, F. Berto, D. Kujawski, Non-linear models for assessing the fatigue crack behaviour under cyclic biaxial loading in a cruciform specimen, *Theor. Appl. Fract. Mech.* 100 (2019) 14–26.
- [31] ASTM E139-11, Standard test methods for conducting creep, creep-rupture, and stress-rupture tests of metallic materials.
- [32] ASTM E647-08e1, Standard test methods for measurements of fatigue crack growth rates.
- [33] Razak N. Ab, C.M. Davies, K.M. Nikbin, Creep-fatigue crack growth behaviour of P91 steels. ECF21, *Procedia Struct. Integrity* (2016) 855–862.
- [34] A.H. Noroozi, G. Glinka, S. Lambert, A two parameter driving force for fatigue crack growth analysis, *Int. J. Fatigue* 27 (2005) 1277–1296.
- [35] A.H. Noroozi, G. Glinka, S. Lambert, A study of the stress ratio effects on fatigue crack growth using the unified two-parameter fatigue crack growth driving force, *Int. J. Fatigue* 29 (2007) 1616–1633.
- [36] P.J. Huffman, A strain energy based damage model for fatigue crack initiation and growth, *Int. J. Fatigue* 88 (2016) 197–204.
- [37] T.M. Edmunds, J.R. Willis, Matched asymptotic expansions in non-linear fracture mechanics-iii. In-plane loading of an elastic perfectly plastic symmetric specimen, *J. Mech. Phys. Solids* 25 (1977) 423–455.
- [38] A. de-Andrés, J.L. Pérez, M. Ortiz, Elastoplastic finite element analysis of three-dimensional fatigue crack growth in aluminum shafts subjected to axial loading, *Int. J. Solids Struct.* 36 (1999) 2231–2258.
- [39] P. Towashiraporn, G. Subbarayan, C.S. Desai, A Hybrid Model for Computationally Efficient Fatigue Fracture Simulations at Microelectronic Assembly Interfaces, *Int. J. Solids Struct.* 42 (2005) 4468–4483.
- [40] J.Z. He, G.Z. Wang, S.T. Tu, F.Z. Xuan, Effects of side-groove depth on creep crack-tip constraint and creep crack growth rate in C(T) specimens, *Fatigue Fract. Eng. Mater. Struct.* 41 (2) (2018) 260–272.
- [41] ASTM E1457-00. Standard Test Method for Measurement of Creep Crack Growth Rates in Metals.